



# Evidence for a more extensive Greenland Ice Sheet in southwestern Greenland during the Last Glacial Maximum

Christopher M. Sbarra<sup>1</sup>, Jason P. Briner<sup>1</sup>, Brandon L. Graham<sup>1</sup>, Kristin Poinar<sup>1</sup>, Elizabeth K. Thomas<sup>1</sup>, and Nicolás E. Young<sup>2</sup>

<sup>1</sup>Department of Geology, 126 Cooke Hall, University at Buffalo, Buffalo, New York 14260, USA

<sup>2</sup>Lamont-Doherty Earth Observatory, Columbia University, 61 Route 9W, Palisades, New York 10964, USA

## ABSTRACT

The maximum extent and elevation of the Greenland Ice Sheet in southwestern Greenland during the Last Glacial Maximum (LGM, 26–19.5 ka) is poorly constrained. Yet, the size of the Greenland Ice Sheet during the LGM helps to inform estimates of past ice-sheet sensitivity to climate change and provides benchmarks for ice-sheet modeling. Reconstructions of LGM ice extents vary between an inner continental shelf minimum, a mid-shelf position, and a maximum extent at the shelf break. We use three approaches to resolve LGM ice extent in the Sisimiut sector of southwestern Greenland. First, we explore the likelihood of minimum versus maximum Greenland Ice Sheet reconstructions using existing relative sea-level data. We use an empirical relationship between marine limit elevation and distance to LGM terminus established from other Northern Hemisphere Pleistocene ice sheets as context for interpreting marine limit data in southwestern Greenland. Our analysis supports a maximum regional Greenland Ice Sheet extent to the shelf break during the LGM. Second, we apply a simple 1-D crustal rebound model to simulate relative sea-level curves for contrasting ice-sheet sizes and compare these simulated curves with existing relative sea-level data. The only realistic ice-sheet configuration resulting in relative sea-level model-data fit suggests that the Greenland Ice Sheet terminated at the shelf break during the LGM. Lastly, we constrain the LGM ice-sheet thickness using cosmogenic <sup>10</sup>Be, <sup>26</sup>Al, and <sup>14</sup>C exposure dating from two summit areas, one at 381 m above sea level at the coast, and another at 798 m asl 32 km inland. Twenty-four cosmogenic radionuclide measurements, combined with results of our first two approaches, reveal that our targeted summits were likely ice-covered during the LGM and became deglaciated at ca. 11.6 ka. Inventories of in situ <sup>14</sup>C in bedrock at one summit point to a small degree of inherited <sup>14</sup>C and suggest that the Greenland Ice Sheet advanced to its maximum late Pleistocene extent at 17.1 ± 2.5 ka. Our results point to a configuration where the southwestern part of the Greenland Ice Sheet reached its maximum LGM extent at the continental shelf break.

## 1. INTRODUCTION

Reconstructions of past ice-sheet dimensions serve as important prescribed features in transient climatic model simulations (He et al., 2013; Zweck and Huybrechts, 2005) and are also used to independently assess paleo-ice-sheet model performance (Downs et al., 2020; Lecavalier et al., 2014; Tarasov and Peltier, 2004). Yet, such reconstructions

Jason Briner <https://orcid.org/0000-0002-8584-0978>

reveal conflicting estimates of the maximum size of the Greenland Ice Sheet during the Last Glacial Maximum (LGM, 26–19.5 ka) around some parts of Greenland. For example, while most reconstructions of Greenland Ice Sheet extent during the LGM depict a terminus located somewhere on the continental shelf, its exact position is uncertain (Fig. 1; Bradley et al., 2018; Fleming and Lambeck, 2004; Funder et al., 2011; Lecavalier et al., 2014). Placing direct constraints on the LGM ice extent requires offshore geophysical surveys, seafloor mapping,

and sediment coring; however, only a few areas have yielded detailed knowledge about past ice extent (Dowdeswell et al., 2014; Hogan et al., 2016; Jennings et al., 2017; Newton et al., 2017; Ó Cofaigh et al., 2013; Ó Cofaigh et al., 2004).

Offshore LGM ice extent can also be inferred using terrestrial evidence. Glacial sediments and landforms can be used to constrain former ice extent, but these archives rarely extend back into the LGM on Greenland (Håkansson et al., 2007; Larsen et al., 2018; Young et al., 2020). Relative sea-level curves have been used in combination with glacially weathered trimlines to infer the size and lateral extent of ice sheets, but these estimates are typically used as a minimum ice-sheet estimate (Funder and Hansen, 1996). A growing number of Greenland's coastal regions have been studied using cosmogenic nuclide exposure dating, which provides absolute age constraints on the timing of ice retreat onto land (e.g., Winsor et al., 2015; Roberts et al., 2009; Søndergaard et al., 2020). However, deglaciation chronologies are less straightforward when used in areas where frozen bedded conditions dominated during the LGM, such as in eastern and northern Greenland, or elsewhere at higher elevations (Briner et al., 2013; Corbett et al., 2013; Graham et al., 2019; Kelly, 1980).

Southwestern Greenland has an extensive terrestrial record of the Greenland Ice Sheet during the Holocene (Young et al., 2020), but like other regions in Greenland, its glacial extent during the LGM is unclear. A commonly cited reconstruction places the southwestern Greenland Ice Sheet LGM terminus a mere 40 km offshore of the modern-day coastline (Funder et al., 2011), yet studies on the wide continental shelf off Disko Bugt support an LGM ice limit at the shelf break (Ó Cofaigh et al.,

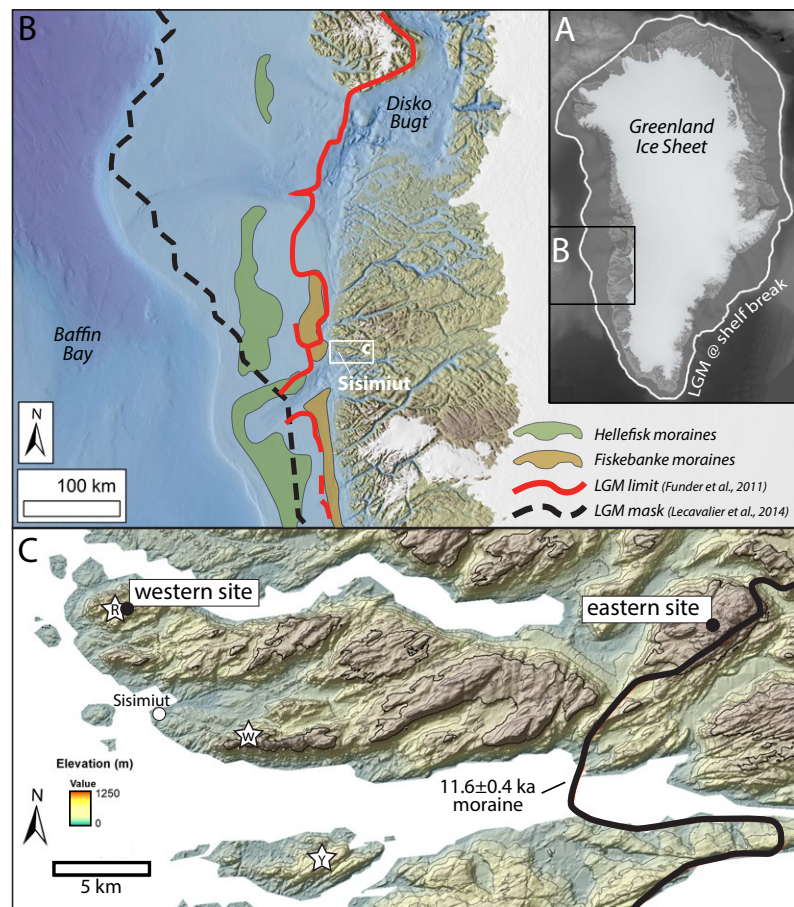


**Figure 1.** (A) Inset map of Greenland. (B) Map shows inferred Last Glacial Maximum (LGM) ice margins and moraine belts on the West Greenland shelf. The black dashed line depicts the LGM terminus in the HUY3 model in Lecavalier et al. (2014); note that it differs significantly from the LGM depiction in Funder et al. (2011) shown in red, yet is supported off of Disko Bugt by field reconstructions (Ó Cofaigh et al., 2013). (C) Locations of our western and eastern samples sites; the black solid line marks the Taserqat Moraine ( $11.6 \pm 0.4$  ka; position from Lesnek et al., 2020; age from Young et al. (2020). Stars with R, W, and Y refer to previous studies Rinterknecht et al. (2009), Winsor et al. (2015), and Young et al. (2020), respectively.

2013). Terrain in southwestern Greenland above ~650 m above sea level (asl) is often heavily weathered and has apparent  $^{10}\text{Be}$  exposure ages that far exceed the LGM period (Kelly and Bennike, 1985; Rinterknecht et al., 2009; Roberts et al., 2009;

Winsor et al., 2015). These results have been interpreted to indicate that the surface of the LGM may not have been more than 650 m asl, which would mean that some mountain summits survived as nunataks during the LGM.

The exposure history of summits interpreted to be potential nunataks could be complicated by non-erosive LGM ice cover. For example, weathered uplands, even those with pre-LGM cosmogenic nuclide inventories in bedrock, and sometimes even in erratics, have been shown to be at least intermittently covered by ice during the LGM (Briner et al., 2006; Corbett et al., 2013; Young et al., 2018). In southwestern Greenland, if coastal uplands were covered by ice during the LGM, it would point to a terminus position far onto the continental shelf and possibly at the shelf break. These issues collectively have led to an uncertain reconstruction of the lateral extent and maximum elevation of the Greenland Ice Sheet during the LGM in some areas around Greenland.

Here, we provide new evidence to support an extensive Greenland Ice Sheet configuration in southwestern Greenland during the LGM. We investigate the relationship between the elevation of marine limits and their locations relative to LGM ice extent. Next, we develop a 1-D crustal rebound model for a model-data comparison of relative sea-level history. Finally, we constrain ice thickness with cosmogenic nuclide measurements from erratic and bedrock surfaces atop coastal summits in southwestern Greenland. Combined, our data suggest that the southwestern Greenland Ice Sheet terminus extended to the shelf break during the LGM.

## 2. BACKGROUND AND METHODS

### 2.1. Marine Limit Data Compilation

Raised marine deposits in deglaciated environments provide valuable information for understanding former ice-sheet loading and post-glacial uplift history (Peltier, 1998). Early work showed that marine limit elevation ( $U$ ) is generally related to its distance from the LGM ice-sheet margin (Andrews, 1968a, 1968b; Andrews et al., 1970; Andrews, 1975). This relationship is:

$$U = C \left( \frac{4 \tau_{av}}{3 \rho_{ice} g} \right) (L - x)^n \quad (1)$$

where the independent variable  $x$  is the distance from the ice center,  $C$  is a constant with a value

near 1,  $L$  is the distance from the ice margin to the center of the ice sheet during the LGM (Andrews, 1968a),  $\tau_{av}$  is the average basal shear stress under an ice sheet with density  $\rho_{ice} = 917 \text{ kg/m}^3$ ,  $g$  is the gravitational acceleration, and  $n$  is an exponent with value near 0.5 (Andrews, 1968a). We fit  $n$  in Equation 1 to the marine limit data using a power trendline.

We explore the relationship between marine limit elevation and its distance to ice-sheet margins by compiling marine limit data from around the Laurentide, Fennoscandia, Barents–Kara, and Greenland Ice Sheets. We use LGM ice-sheet outlines from published compilations (Funder et al., 2011; Dalton et al., 2020; Hughes et al., 2016) and include 62 marine limit observations from northeastern Canada (Dyke et al., 2005), 55 from Greenland, 22 from Svalbard (Forman, 1990), and 42 from Ireland, the UK, and Scandinavia (Hogan et al., 2016) (Fig. 2). We measure the distance from each marine limit location to the mapped LGM ice-sheet margin. In places where the mapped LGM

extent did not reach the shelf break, we made a second measurement from the marine limit location to the shelf break.

## 2.2. One-Dimensional Crustal Rebound Model and Simulated Relative Sea-Level Curves

We compare observations of marine limit elevations and relative sea level with results from a simple model run with contrasting Greenland ice-loading scenarios. To do so, we applied a simple 1-D crustal rebound model to incorporate ice-sheet profiles calculating the ice-sheet thickness,  $H$ , at a given distance,  $x$ , from the margin (van der Veen, 2013):

$$H(x) = \left( \frac{2 \tau_y}{\rho_{ice} g} x \right)^{0.5} \quad (2)$$

where  $\tau_y$  is the yield stress. Discretization of Equation 2 using the forward Euler method along a

roughly flow-parallel transect allows calculation of the ice-sheet surface elevation,  $h_i$ , at discrete positions,  $x_i$ , from the margin, where  $i$  represents the index of discretization and  $\Delta x$  the spatial step:

$$h_{i+1} = h_{i+1}^2 - h_{i+1}(B_i + B_{i+1}) + h_i(B_{i+1} - H_i) - \left( \frac{2 \Delta x \tau_y}{\rho_{ice} g} \right) \quad (3)$$

following Benn and Hulton (2010) and using bed elevations  $B$  from Morlighem et al. (2017). We constrained the yield stress by applying Equation 3 to a transect from the modern ice divide to the modern terminus and tuning the yield stress until the surface elevation profile  $h(x)$  best matched the current ice-sheet surface profile from Morlighem et al. (2017). We found a best-fit yield stress of 110 kPa, which we employed at all paleo-model times. This model represents the Greenland Ice Sheet as a land-terminating ice sheet, although in both paleo scenarios, it was likely marine-terminating (Fig. 3).

We modeled two versions of the ice sheet, one with an LGM terminus at the shelf break (“Max Ice”)

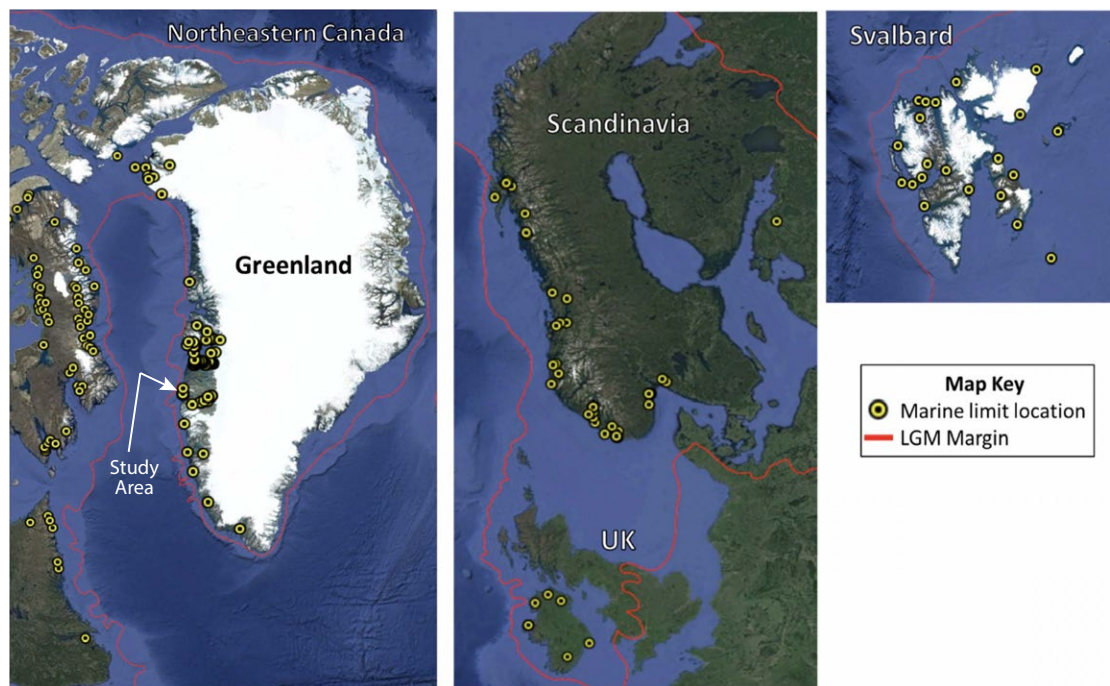


Figure 2. Marine limit data (yellow dots) assembled from the literature (see text) and Last Glacial Maximum (LGM) ice margins (red lines) from Dalton et al. (2020) and Hughes et al. (2016) are shown. Map backgrounds are from Google Earth; data sources are U.S. Geological Survey, SIO, NOAA, U.S. Navy, NGA, GEBCO, IBCAO, Landsat/Copernicus.

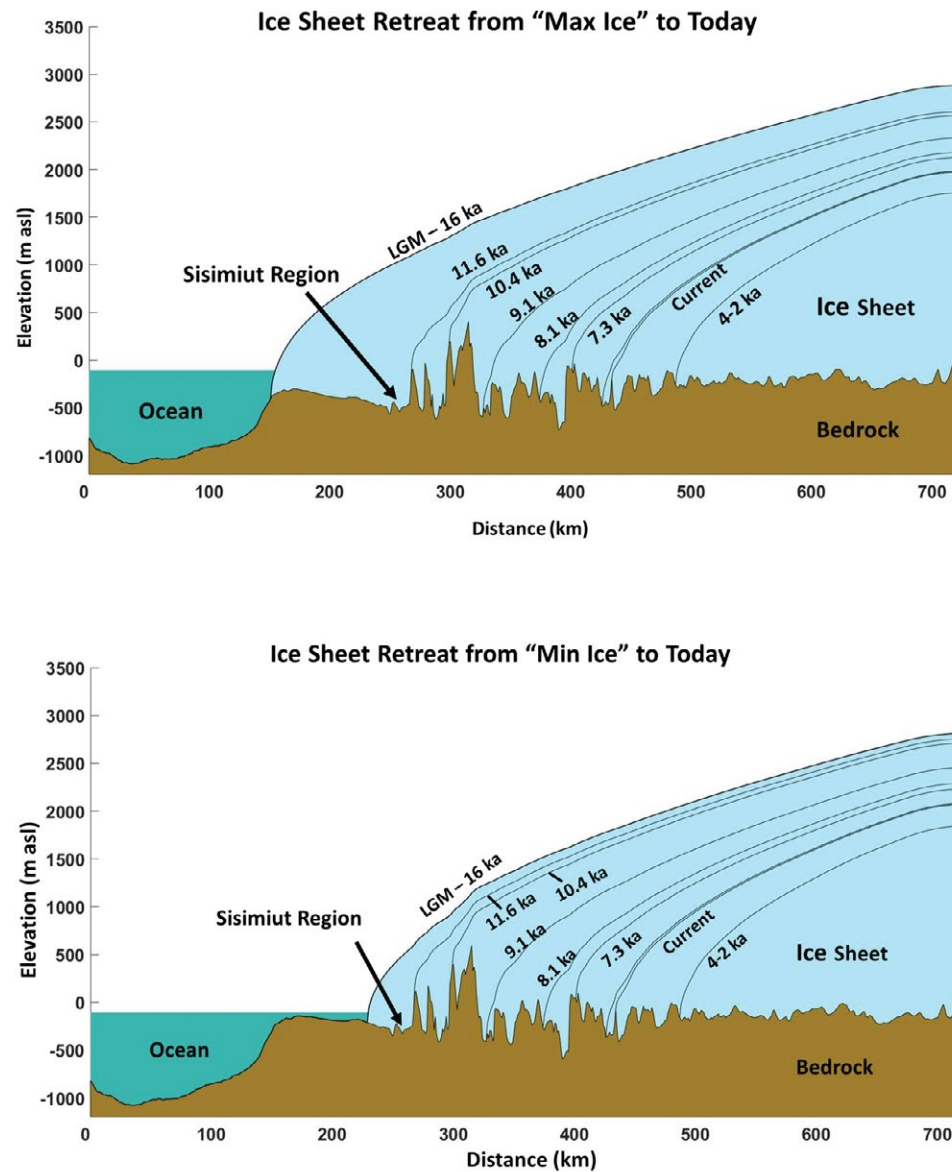


Figure 3. (Top) “Max Ice” Greenland Ice Sheet profile shows full isostatic depression during the Last Glacial Maximum (LGM) in the Sisimiut region. (Bottom) “Min Ice” Greenland Ice Sheet profile during the LGM. Both scenarios show ice sheet profiles throughout the Holocene. The bedrock and ocean are at their LGM elevations in both images, although they rebound as ice retreats in the model.

and another with the LGM terminus at the location at the Fiskebanke moraines on the inner shelf (“Min Ice” in Fig. 3). We enforced these configurations from 30 ka until 15 ka, which was long enough to relax the underlying crust into equilibrium with the overlying ice load. We applied the same retreat history to both the Max Ice and Min Ice configurations. We initiated deglaciation at 15 ka based on the timing of retreat from the shelf break farther north (e.g., Ó Cofaigh et al., 2013) and then used five mapped Greenland Ice Sheet margin positions for Holocene time steps at 11.6 ka, 10.4 ka, 9.1 ka, 8.1 ka, and 7.3 ka based on data from Young et al. (2020) and Lesnek et al. (2020), with linear retreat rates between each ice margin position. There is evidence that the Greenland Ice Sheet retreated inland of its current position during the middle Holocene. Although the exact distance remains unknown, it likely was no more than a few tens of kilometers from its current position (Young et al., 2021; Lesnek et al., 2020; Ruskeeniemi et al., 2018; Young and Briner, 2015). We represented this by positioning the margin at the modern terminus at 5.5 ka, then 20 km inland of the modern terminus from 4.0 ka to 1.2 ka, then at its modern position at 0 ka, with linear rates of margin migration between these defined times.

For each configuration of the ice sheet at the LGM, we subtracted the local thickness of the modern ice sheet to obtain a thickness change,  $\Delta H$ , along our transect. We used  $\Delta H$  to calculate the visco-elastic displacement of the crust during the LGM using the modern topography as a baseline (Morlighem et al., 2017). Our simple model represents the lithosphere as an elastic beam floating in the mantle, following the classic bending beam problem modeled with the biharmonic equation that was outlined and solved by Turcotte and Schubert (2002). At every model timestep, we calculated the elastic displacement of the crust  $w_e(x)$ :

$$w_e(x) = \frac{v(x) \alpha^3}{8 D} \quad (4)$$

where  $D$  is the flexural rigidity parameter for the lithosphere, defined below, which is weighted by a spatially varying line load,  $v(x)$ , that represents the ice sheet:

$$v(x) = g \rho_{ice} H(x) \Delta x \quad (5)$$

where we represent the ice sheet as a series of line loads of width  $\Delta x = 500$  m, spatially varying thickness,  $H(x)$ , and ice density,  $\rho_{ice}$  of  $917 \text{ kg/m}^3$ . The horizontal length scale of the forebulge,  $\alpha$ , is defined as:

$$\alpha = \left( \frac{4D}{\rho_m g} \right)^{\frac{1}{4}} \quad (6)$$

where mantle density,  $\rho_m$ , is  $3200 \text{ kg/m}^3$ . The flexural rigidity parameter  $D$  is:

$$D = \frac{Ed^3}{12(1-\nu^2)} \quad (7)$$

where the Young's modulus of the elastic lithosphere  $E$  is 70 GPa (Turcotte and Schubert, 2002), the lithospheric elastic thickness  $d$  is 80 km (Steffen et al., 2018), and Poisson's ratio  $\nu$  for ice is 0.25 (Turcotte and Schubert, 2002). Our crustal model produces a maximum subglacial depression ( $\sim -630$  m), a slight proglacial depression immediately beyond the terminus ( $\sim -130$  m), and a forebulge ( $\sim +15$  m) at a distance of  $\alpha \sim 150$  km beyond the terminus.

We also model the viscous response of the lithosphere to the loading and unloading by advance and retreat of the ice sheet. The timescale of this response,  $T_r$ , is:

$$T_r = \frac{4 \pi \mu}{\rho_m g L} \quad (8)$$

where  $\mu$  is the viscosity of the upper mantle ( $5 \times 10^{20} \text{ Pa} \cdot \text{s}$ ) (Wake et al., 2016) and  $L$  is the length of the LGM ice sheet (Meinesz, 1937). With these physical constants and the differing ice-sheet lengths  $L$  in the "Max Ice" and "Min Ice" configurations, we find that  $T_r$  for the "Max Ice" model is 4300 yr and  $T_r$  for the "Min Ice" model is 6200 yr.

We model the time evolution of the viscous displacement of the crust,  $w(t)$ , as exponential decay:

$$w(t) = w_{max} e^{-\frac{t}{T_r}} \quad (9)$$

where  $w_{max}$  is the depression of the bed during the LGM. This model allows the crust to rebound as soon as the ice sheet begins to thin, even when still covered in ice (i.e., restrained rebound).

To validate this simple model for visco-elastic deformation of the lithosphere, we ran the Benchmark A comparison test described in Martinec et al.

(2018) and Spada et al. (2011). Our modeled vertical displacement under the outer 70% of the glaciated area agreed with the Benchmark A results (Martinec et al., 2018) to within 10 m ( $\sim 10\%$ ).

Eustatic sea level increased simultaneously with ice-sheet retreat (Lambeck et al., 2014). We calculate the relative sea level at a site at a given time,  $R(t)$ , over the entire model duration (pre-15 ka to present) as follows:

$$R(t) = B_0 - B(t) + S(t) \quad (10)$$

where  $B_0$  is the modern crust elevation (Morlighem et al., 2017),  $B(t)$  is the elevation of the crust at a given time, and  $S(t)$  is global sea level at a given time (Lecavalier et al., 2014). This allows us to simulate a relative sea-level curve for a selected site spanning from deglaciation to today (Fleming et al., 1998).

### 2.3. Cosmogenic-Nuclide Exposure Dating

Three previous studies with cosmogenic nuclide measurements are relevant to our work because they include  $^{10}\text{Be}$  ages in the Sisimiut area. Here, we recalculated published ages using the methods described below. Samples collected from bedrock above 650 m asl yielded some ages in excess of 100 ka (Roberts et al., 2009), and samples from lower elevations have  $^{10}\text{Be}$  ages that are  $>15$  ka and thus could be interpreted to indicate ice-free LGM conditions or early deglaciation (Rinterknecht et al., 2009; Roberts et al., 2009). Roberts et al. (2009) interpreted a boundary at  $\sim 650$  m asl as a possible maximum LGM ice-sheet elevation for the region and supported a limited maximum lateral extent with the LGM terminus placed just offshore (Kelly and Bennike, 1985; Weidick and Bennike, 2007). Winsor et al. (2015) reported ages of ca. 35 ka from boulders at  $\sim 600$  m asl, which could be interpreted to indicate an even lower LGM ice surface. Winsor et al. (2015) also reported  $^{10}\text{Be}$  ages of boulders that average ca.  $14.5 \pm 1.0$  ka from  $\sim 150$  m asl and suggested that deglaciation of the Sisimiut area took place at this time. The ca. 14.5 ka age of deglaciation in Winsor et al. (2015) contrasts with a single  $^{10}\text{Be}$  age of ca. 20 ka from a boulder at  $\sim 400$  m

asl only  $\sim 10$  km away reported by Rinterknecht et al. (2009). Finally, Young et al. (2020) reported three  $^{10}\text{Be}$  ages from  $\sim 230$  m asl that average  $11.5 \pm 0.3$  ka, which is notably younger than the nearby ages from Winsor et al. (2015). All of these previously dated sites lie to the west of the Taserqat Moraine, which Young et al. (2020) dated to  $11.6 \pm 0.4$  ka ( $n = 5$ ).

To further explore the unresolved nature of upland glaciation and former Greenland Ice Sheet thickness in the Sisimiut area, we use multiple nuclides,  $^{10}\text{Be}$ ,  $^{26}\text{Al}$ , and in situ  $^{14}\text{C}$ , due to their combined utility in elucidating glacier history in areas with complex exposure histories (e.g., Beel et al., 2016; Bierman et al., 1999; Graham et al., 2019; Young et al., 2018). We collected three bedrock and six boulder samples from a summit adjacent to the ocean with sample elevations ranging from 355 m asl to 397 m asl (Figs. 4–5). The summit at this "western site" displays evidence of past ice cover due to the presence of glacial erratics. Signs of advanced subaerial weathering, such as protruding quartz veins with  $\sim 1$ – $2$  cm of relief above the surrounding bedrock, are also visible at this site, which indicates a potentially complex exposure history. We also collected three bedrock samples from a summit at 798 m asl located 32 km inland from the western site (Figs. 4–5). The summit bedrock surfaces at this "eastern site" exhibit signs of advanced weathering with deep weathering pits; no boulders suitable for sampling were present.

We collected samples using a rock hammer, chisel, and angle grinder from the top  $\sim 2$  cm of each surface. The boulders were perched in positions that imply stability since deposition. Bedrock samples were collected from local topographic high points to minimize the effect of shielding from seasonal snow cover and surrounding topography.

We processed samples using a series of physical and chemical treatments. At the University at Buffalo (Buffalo, New York, USA), the rock samples were crushed and then sieved to 250–500  $\mu\text{m}$ . Quartz was isolated using froth flotation in an acetic acid solution followed by hydrochloric and hydrofluoric/nitric acid baths. We dissolved clean quartz with beryllium carrier with a concentration of 1074 ppm of  $^9\text{Be}$  and added  $^{26}\text{Al}$  carrier (1001 ppm)

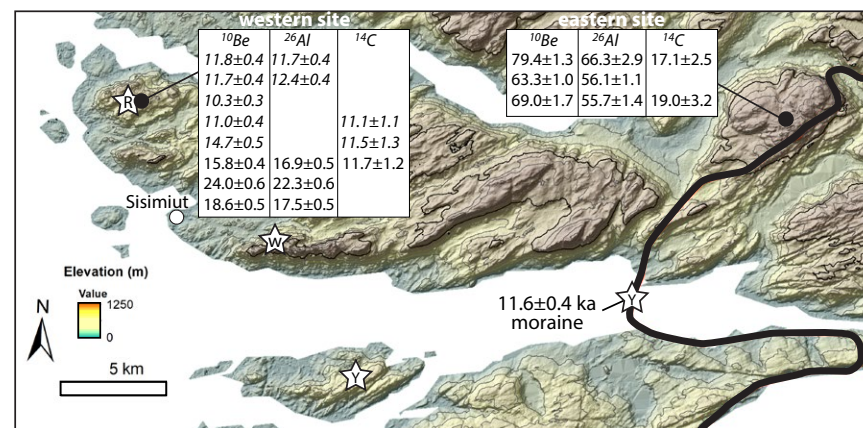


**Figure 4.** Location of the western and eastern sites in the Sisimiut region is shown (black dots with ages). GRE-1 from Rinterknecht et al. (2009) (star with “R”;  $19.6 \pm 5.2$  ka) is from the same erratic boulder as sample 18GRO-9 from this study ( $11.0 \pm 0.4$  ka). Sample areas from other publications (stars) include Winsor et al. (2015; “W”) and Young et al. (2020; “Y”). Italicized ages are from boulders; non-italicized ages are from bedrock surfaces.

to the bedrock samples (Corbett et al., 2016). Once beryllium and aluminum were isolated and purified, they were oxidized and loaded into cathodes for accelerator mass spectrometry (AMS) measurement at PRIME Lab at Purdue University (West Lafayette, Indiana, USA). <sup>10</sup>Be and <sup>26</sup>Al ages were calculated with the CRONUS v3 online age calculator (<https://hess.ess.washington.edu>), and <sup>10</sup>Be and <sup>26</sup>Al ages were calculated using the Baffin Bay production rate of Young et al. (2013) using the Lm scaling scheme (Balco et al., 2008; Lal, 1991; Stone, 2000). We also processed six quartz separates for in situ <sup>14</sup>C analysis at Lamont-Doherty Earth Observatory following standard procedures detailed in Lamp et al. (2019). To avoid potential carbon contamination from the froth flotation procedure at the University at Buffalo, we leached samples in concentrated nitric acid for several days before processing them further. The measured <sup>14</sup>C concentrations were blank-corrected using a long-term laboratory blank (Lamp et al., 2019). In situ <sup>14</sup>C ages were calculated using the western Greenland (<sup>14</sup>C) production rate calibration data set (Young et al., 2014) and Lm scaling (Balco et al., 2008; Lal, 1991; Stone, 2000).

## 3. RESULTS AND INTERPRETATION

### 3.1. Marine Limit Data Complication

Our marine limit analysis shows that marine limit elevation is significantly related to distance from the hypothesized LGM margin (Fig. 6). We fit data for all four ice sheets to Equation 1 and found  $r^2 = 0.73$  with  $C = 4.7$  and  $n = 0.50$  in agreement with the theoretical value of  $n = 0.5$  and  $C$  of order 1 (Andrews, 1968a). Some of the scatter, we assume, is due to the added influence that ice margin history during deglaciation (variable retreat rate, stillstands, and re-advances) has on the relationship. Of particular interest are the data from southwestern Greenland using the Greenland Ice Sheet ice limit from Funder et al. (2011), which fall outside the trend of data from all other ice sheets (Fig. 6). On the other hand, when using an LGM margin at the shelf break, the best-fit equation resembles that of other ice sheets much more closely.

The LGM reconstruction of Greenland Ice Sheet extent in the Sisimiut region proposed by Dyke (2004) and Funder et al. (2011) results in a marine limit versus distance relationship that differs from

that of other Northern Hemisphere ice sheets (Fig. 6) and requires a relationship different from the theoretical parabolic profile (Equation 1). On the other hand, our “Max Ice” scenario, in which the ice-sheet terminus reaches the shelf break, the marine limit versus distance plot becomes similar to the results from other ice sheets (Fig. 6) and fits well with a parabolic profile. These findings support an LGM extent at the shelf break off Sisimiut.

### 3.2. Crustal Rebound Model

The results from our crustal rebound simulations (see animations in Supplemental Material<sup>1</sup>) show relative sea-level histories similar to those from independent observations. Our simulated relative sea-level curve using “Max Ice” and a deglaciation age of 12 ka yields a marine limit for Sisimiut of 136 m asl. This is close to the observed marine limit of 140 m asl and generally compatible with field constraints of relative sea level (Bennike et al., 2011; Funder and Hansen, 1996; Long et al., 2011). The simulated marine limit using “Min Ice” is 47 m asl and has a poorer fit with observations (Fig. 7). Thus, the overall better fit between our simulated “Max Ice” relative sea-level history and observations favors a “Max Ice” scenario.

Despite the agreement between geological observations and the results from our “Max Ice” crustal rebound simulations, the ice-sheet history we use in our model is not well constrained prior to 11.6 ka. In our “Max Ice” scenario, we force the ice margin to retreat from the continental shelf break at 15 ka (see Section 2.2) and then prescribe a linear retreat rate over the next 4.4 k.y. until the ice margin reaches the next recorded position ~115 km inland at 11.6 ka. In our “Min Ice” scenario, we also begin retreat at 15 ka at a constant rate until 11.6 ka, but the ice margin begins much farther inland (Fig. 3). If the Greenland Ice Sheet had a complex ice-margin history with cycles of repeated advance and retreat (e.g., retreat

<sup>1</sup>Supplemental Material. Animations of ice-sheet recession and crustal rebound for minimum and maximum LGM ice sheet configurations. Please visit <https://doi.org/10.1130/GEOS.S19469402> to access the supplemental material, and contact editing@geosociety.org with any questions.



Figure 5. Photographs of selected samples show cosmogenic nuclide exposure ages and one standard deviation error (in ka).

from the LGM limit during the Bølling followed by re-advance and final retreat after the Younger Dryas), such an ice-margin history could lead to a different loading history. Similarly, our assumption that the crust achieved equilibrium with the LGM ice load may not be valid if the Greenland Ice Sheet was at its maximum extent for a relatively short period, such as arriving to its LGM limit not long before it receded from that limit, a result that is supported by

our cosmogenic nuclide results (see Section 3.3). If the maximum LGM ice extent were reached relatively late and occupied for only a brief period of time, then the Greenland Ice Sheet would need to have been thicker than in our “Max Ice” simulation to yield a marine limit that matches independent observations. In any case, despite these uncertainties, our simplified ice-sheet history for “Max Ice” nevertheless produced a reasonably close fit with observations (Fig. 7).

We also explored how thick the Greenland Ice Sheet would have to be in our “Min Ice” scenario to reproduce the observed 140 m asl marine limit near Sisimiut. This requires an ice thickness of ~1400 m at the modern coastline, which would require an increase in the yield stress from 110 kPa to 310 kPa to maintain an inner-shelf terminus position. In addition to being a factor of three higher than the typically accepted value (van der Veen, 2013), a yield stress of 310 kPa results in an ice-sheet thickness over 5 km at the ice divide. We find it unlikely that a minimum ice configuration could result in a reasonable data-model fit.

### 3.3. Cosmogenic Nuclide Concentrations

From the western site, three bedrock samples have  $^{10}\text{Be}$  ages of  $24.0 \pm 0.6$  ka,  $18.6 \pm 0.5$  ka, and  $15.8 \pm 0.4$  ka (Tables 1–2). The five samples from erratics at the western site have  $^{10}\text{Be}$  ages of  $14.7 \pm 0.5$  ka,  $11.8 \pm 0.4$  ka,  $11.7 \pm 0.4$  ka,  $11.0 \pm 0.4$  ka, and  $10.3 \pm 0.3$  ka. The  $^{26}\text{Al}$  ages at the western site are in good agreement with the  $^{10}\text{Be}$  ages, and the  $^{26}\text{Al}/^{10}\text{Be}$  ratios of the samples range from  $6.77 \pm 0.26$ – $7.78 \pm 0.31$  (Table 1). We measured in situ  $^{14}\text{C}$  in four samples from the western site (one bedrock and three erratics) to further constrain the exposure history of the site (Table 2). In situ  $^{14}\text{C}$  ages from two erratics are  $11.1 \pm 1.1$  ka and  $11.5 \pm 1.4$  ka, and the bedrock sample has an age of  $11.7 \pm 1.2$  ka. One of the in situ  $^{14}\text{C}$  measurements from an erratic resulted in a concentration of ~210 k atoms/g, which is higher than the site-specific saturation value of ~190 k atoms/g. We suspect this sample was contaminated during the extraction process and disregard it from further consideration.

Two of the erratic samples (18GRO-6 and 18GRO-11) at the western site have  $^{10}\text{Be}$  ages that are beyond the  $1\sigma$  age range of the others (one older, one younger; Fig. 4), and the average age of the remaining three erratics is  $11.5 \pm 0.4$  ka. We interpret this age of  $11.5 \pm 0.4$  ka as the timing of deglaciation at the western site.

The in situ  $^{14}\text{C}$  ages for the samples from the western site strengthen the case for the  $11.5 \pm 0.4$  ka age best representing the timing of deglaciation.

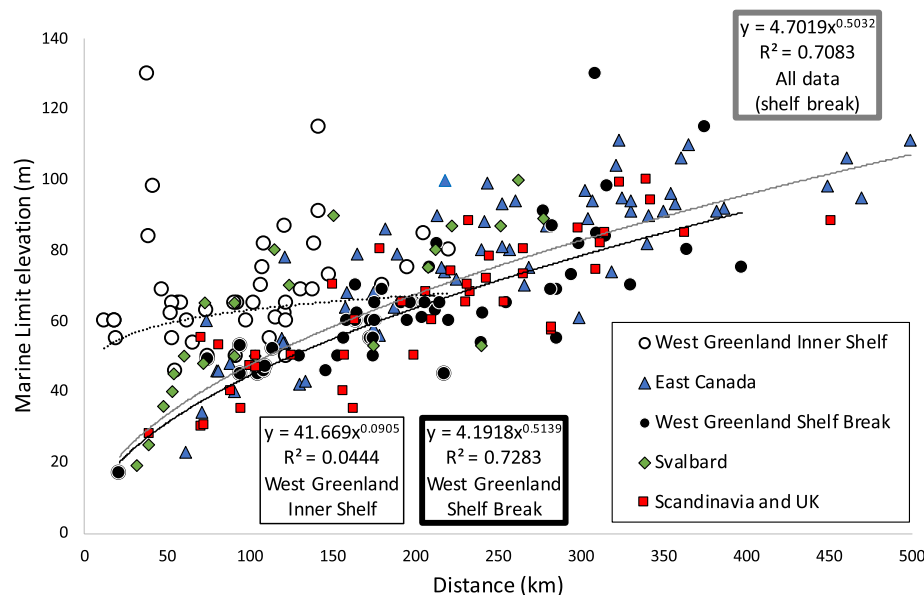


Figure 6. Marine limit elevation versus distance to Last Glacial Maximum (LGM) ice margin is shown. The south-western Greenland data plotted using an inner shelf LGM limit (Funder et al., 2011) are shown as white circles; the same data using an LGM limit at the shelf break are re-plotted as black circles.

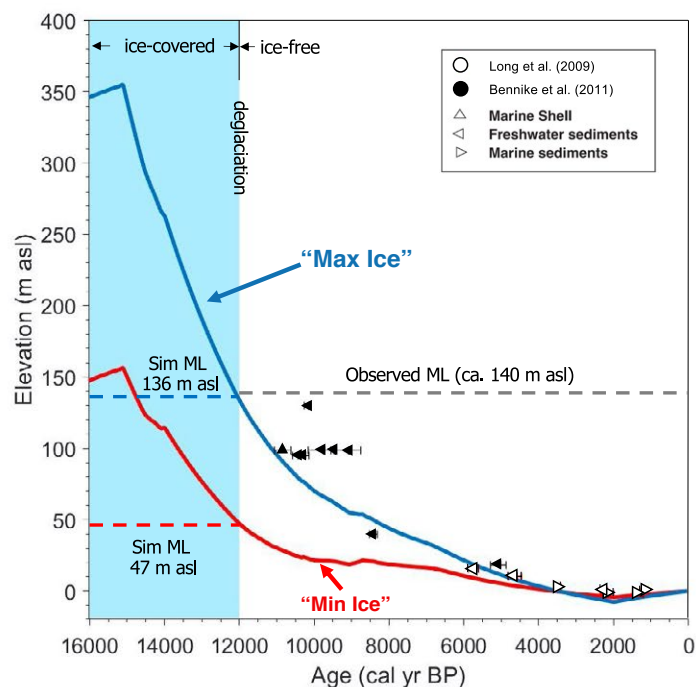


Figure 7. Relative sea-level observations at Sisimiut are compared to modeled relative sea-level curve and marine limit elevations for “Max Ice” and “Min Ice.” The blue area shows when the location was covered in ice. Black-filled symbols are from Bennike et al. (2011); white-filled symbols are from Long et al. (2009). Sim—simulated; ML—marine limit.

Sample 18GRO-9, an erratic with a  $^{10}\text{Be}$  age of  $11.0 \pm 0.4$  ka, has an in situ  $^{14}\text{C}$  age of  $11.1 \pm 1.1$  ka. Both 18GRO-4 (bedrock) and 18GRO-11 (erratic) have  $^{10}\text{Be}$  and  $^{26}\text{Al}$  ages (ca. 15–17 ka) that are older than our interpreted age of deglaciation (ca. 11.5 ka), which we suspect is due to inheritance. The in situ  $^{14}\text{C}$  ages for these same samples (11.7 ka and 11.5 ka, respectively) are within  $1\sigma$  of our erratic  $^{10}\text{Be}$ -based age of deglaciation of  $11.5 \pm 0.4$  ka. The average of all three in situ  $^{14}\text{C}$  ages from the western site is  $11.5 \pm 0.3$  ka, the same as our average age of deglaciation based on  $^{10}\text{Be}$  ages of erratics ( $11.5 \pm 0.4$  ka). Overall, these ages support a deglaciation of the western site around the Younger Dryas/Holocene boundary and imply ice cover prior to that time.

At the eastern site, the three bedrock samples (18GRO-1A, 18GRO-, and 18GRO-2) have  $^{10}\text{Be}$  ages of  $79.4 \pm 1.3$  ka,  $63.3 \pm 1.0$  ka, and  $69.0 \pm 1.7$  ka, with corresponding  $^{26}\text{Al}$  ages of  $66.3 \pm 2.9$  ka,  $56.1 \pm 1.1$  ka, and  $55.7 \pm 1.4$  ka (Table 1; Fig. 4). The three samples have  $^{26}\text{Al}/^{10}\text{Be}$  ratios ranging from  $5.85 \pm 0.20$ – $6.40 \pm 0.16$  ka (Table 1). We also measured in situ  $^{14}\text{C}$  in two of the bedrock samples from the eastern site, which are  $17.1 \pm 2.5$  ka and  $19.0 \pm 3.2$  ka (Table 2; Fig. 4).

The cosmogenic nuclide data from the eastern site exhibit evidence for a complex burial and exposure history. The  $^{26}\text{Al}$  and  $^{10}\text{Be}$  ages from the three bedrock surfaces are far older than the regional timing of deglaciation (e.g., Young et al., 2020). The samples have  $^{26}\text{Al}/^{10}\text{Be}$  ratios that are  $6.10 \pm 0.13$ ,

TABLE 1. SAMPLE INFORMATION FOR <sup>10</sup>Be AND <sup>26</sup>Al AGES FROM THE SISIMIUT REGION, SOUTHWESTERN GREENLAND

Sample ID	Sample type*	Latitude (°N)	Longitude (°E)	Elevation (m asl)	Sample thickness (cm)	<sup>10</sup> Be ± 1 SD (atoms/g)	<sup>26</sup> Al ± 1 SD (atoms/g)	<sup>10</sup> Be age	<sup>26</sup> Al age	<sup>26</sup> Al: <sup>10</sup> Be ratio
<b>Eastern Site</b>										
18GRO-1A	Bedrock	66.99065	53.03299	798	1.5	729219 ± 11480	4414352 ± 184889	79420 ± 1270	66320 ± 2880	6.05 ± 0.27
18GRO-1B	Bedrock	66.99065	53.03299	798	1.5	585295 ± 9434	3746217 ± 74219	63300 ± 1040	56110 ± 1140	6.40 ± 0.16
18GRO-2	Bedrock	66.99126	53.03499	798	1.5	636746 ± 15294	3723723 ± 89003	69030 ± 1690	55650 ± 1370	5.84 ± 0.19
<b>Western Site</b>										
18GRO-3	Erratic (1 × 1.5 × 1)	66.98572	53.73038	355	1.5	73017 ± 2575	524633 ± 19658	11830 ± 420	11660 ± 440	7.18 ± 0.36
18GRO-4	Bedrock	66.9865	53.73306	381	1.5	99861 ± 2505	777310 ± 24112	15800 ± 400	16860 ± 530	7.78 ± 0.31
18GRO-5	Erratic (1 × 1 × 0.5)	66.98761	53.73302	385	1.5	74624 ± 2384	575600 ± 19950	11740 ± 380	12420 ± 430	7.71 ± 0.36
18GRO-6	Erratic (0.5 × 0.5 × 0.3)	66.9876	53.7346	397	1.0	69431 ± 2112		10310 ± 320		
18GRO-7	Bedrock	66.98763	53.73459	397	1.5	152143 ± 4011	1040611 ± 28078	24020 ± 630	22270 ± 610	6.83 ± 0.25
18GRO-8	Bedrock	66.98768	53.73335	386	1.5	118158 ± 3246	811268 ± 21556	18580 ± 510	17540 ± 470	6.86 ± 0.26
18GRO-9	Erratic (1 × 1 × 1)	66.9862	53.7359	376	2.0	72172 ± 2323		11030 ± 360		
18GRO-11	Erratic (1.5 × 1.5 × 1.5)	66.9854	53.7408	388	3.0	96558 ± 3215		14720 ± 490		

Note: For age calculations, we used a rock density of 2.65 g/cm<sup>3</sup>. There was no topographic shielding for any of these samples. We ran these samples in multiple batches; process blanks had <sup>10</sup>Be/<sup>9</sup>Be ratios of 2.025 × 10<sup>-15</sup>, 5.133 × 10<sup>-15</sup>, and 2.980 × 10<sup>-15</sup> and <sup>26</sup>Al/<sup>27</sup>Al ratios of 9.298 × 10<sup>-15</sup> and 15.78 × 10<sup>-15</sup>. SD—standard deviation.

\*Erratic sizes are in H, W, L in meters.

TABLE 2. IN SITU <sup>14</sup>C SAMPLE EXTRACTION DETAILS

Sample	Quartz (g)	Carbon yield (µg C)	Carbon yield unc. (µg C)	Diluted carbon mass (µg C)	Diluted carbon mass unc. (µg C)	Fm	Fm unc.	δ <sup>13</sup> C (‰, VPDB)	<sup>14</sup> C/ <sub>total</sub>	<sup>14</sup> C/ <sub>total,unc</sub>	<sup>14</sup> C concentration (atoms/g)	<sup>14</sup> C concentration unc. (atoms/g)	Blank correction applied (# of atoms)	Blank correction unc. (# of atoms)	Age ka (Lm)	Age ka unc.
18GRO-1A	5.2108	27.77	0.32	51.00	0.60	0.4587	0.0050	-24.6	5.2652E-13	5.7393E-15	241918	10383	85768	12070	17.14	2.47
18GRO-02	5.3878	26.86	0.31	46.73	0.55	0.5245	0.0108	-23.6	6.0328E-13	6.3261E-15	246427	10619	85768	12070	19.04	3.21
18GRO-04	5.3859	15.66	0.18	36.80	0.42	0.4130	0.0054	-26.4	4.7233E-13	6.1757E-15	145885	6739	85768	12070	11.74	1.20
18GRO-05	5.3754	24.85	0.29	42.30	0.50	0.5028	0.0059	-27.0	5.7432E-13	6.7393E-15	210643	9297	85768	12070	NA	NA
18GRO-09	5.3214	20.45	0.24	48.40	0.48	0.2964	0.0038	-17.9	3.4489E-13	4.4217E-15	141162	6311	85768	12070	11.13	1.05
18GRO-11	5.3821	18.03	0.21	38.70	0.32	0.3838	0.0110	-19.4	4.4523E-13	1.2761E-14	144580	7795	85768	12070	11.53	1.35

Note: <sup>14</sup>C concentration uncertainty includes the raw measurement uncertainty and a 3.6% uncertainty propagated through to reflect the Lamont-Doherty Earth Observatory (LDEO) scatter in CRONUS-A measurements (updated from Lamp et al., 2019). Blank correction is the average and 1-sigma standard deviation of five process blank measurements: Blank\_11\_28\_17 (72762 ± 2835), Blank\_11\_1\_18 (78139 ± 4303), Blank\_5\_3\_19 (85328 ± 2334), Blank\_9\_10\_19 (88148 ± 2480), and Blank\_3\_2\_20 (104464 ± 2699). See Young et al. (2021) for details. All samples were measured at Centre de Recherche et d'Enseignement de Géosciences de l'Environnement (CEREGE) (Bard et al., 2015; Tuna et al., 2018). VPDB—Vienna Pee Dee Belemnite carbon isotope standard; Fm—fraction modern; unc.—uncertainty.

significantly lower than 7.3, which has been proposed as an appropriate constant exposure value for high latitudes (Corbett et al., 2017; Halsted et al., 2021). This indicates that these samples experienced episodes of burial, upwards of 250 k.y., likely by overriding ice (Bierman et al., 1999; Beel et al., 2016; Strunk et al., 2017). These durations increase when using a ratio of 7.3. These <sup>26</sup>Al/<sup>10</sup>Be

ratios, which are similar to values that others have found in western Greenland uplands (Roberts et al., 2009; Beel et al., 2016; Corbett et al., 2017), do not allow us to definitively say when this burial occurred, but it is possible that a portion of the burial occurred during the LGM (Beel et al., 2016).

Without further information, whether the eastern site was covered during the LGM remains

unknown. However, the apparent in situ <sup>14</sup>C ages provide additional insight. Samples 18GRO-1a and 18GRO-2 are much younger than their <sup>10</sup>Be and <sup>26</sup>Al ages and average 18.1 ± 1.3 ka. There are two ways that these results could be interpreted. First, the in situ <sup>14</sup>C ages could represent the timing of deglaciation of the eastern site. Second, the ages could contain some amount of inherited <sup>14</sup>C due to only

a brief, minimally erosive overriding event during the LGM, in which case the site was deglaciated sometime after ca. 18.1 ka. In the next section, we explore these interpretations in light of the larger data set from both our data from the western site and prior work.

## 4. DISCUSSION

### 4.1. Support for a More Extensive Greenland Ice Sheet in Southwestern Greenland during the LGM

The cosmogenic nuclide ages at the western site agree with  $^{14}\text{C}$ -dated sediments collected from lakes in the region. Our ages are older than the basal lake  $^{14}\text{C}$  sediment age of 10.5–11.0 cal ka B.P. (re-calibrated) that provides a minimum limiting deglaciation age for the region (Bennike et al., 2011). The deglaciation of the western site also agrees with the average of three  $^{10}\text{Be}$  ages from erratic boulders ( $11.5 \pm 0.3$  ka) collected ~10 km south of Sisimiut reported by Young et al. (2020) (Fig. 4). The  $^{26}\text{Al}/^{10}\text{Be}$  ratios from the western site samples reveal insignificant burial even considering the two pairs from bedrock with low levels of inheritance (Fig. 8). Based on this, we interpret the age of deglaciation for the Sisimiut coast to be ca. 11.5 ka.

We suggest that both the western and eastern sites were deglaciated at around the same time, in which case the in situ  $^{14}\text{C}$  concentrations are likely due to (1) low-magnitude erosion (if any) of the bed due to non-erosive ice conditions during the LGM and/or (2) an insufficient duration of ice cover to result in complete  $^{14}\text{C}$  decay. The 11.6 ka Taserqat Moraine is draped across the massif of the eastern site (Fig. 4), a mere ~100 m lower in elevation than the summit and only ~1 km to the SE. Given this geometry, we find it unlikely that the eastern site would have remained a nunatak during the LGM. Moreover, considering our exposure ages from the western site and across the general field area, we suggest our eastern site likely deglaciated just prior to Taserqat moraine deposition. Both the western site and the island site of Young et al. (2020) deglaciated at ca. 11.5 ka, the same

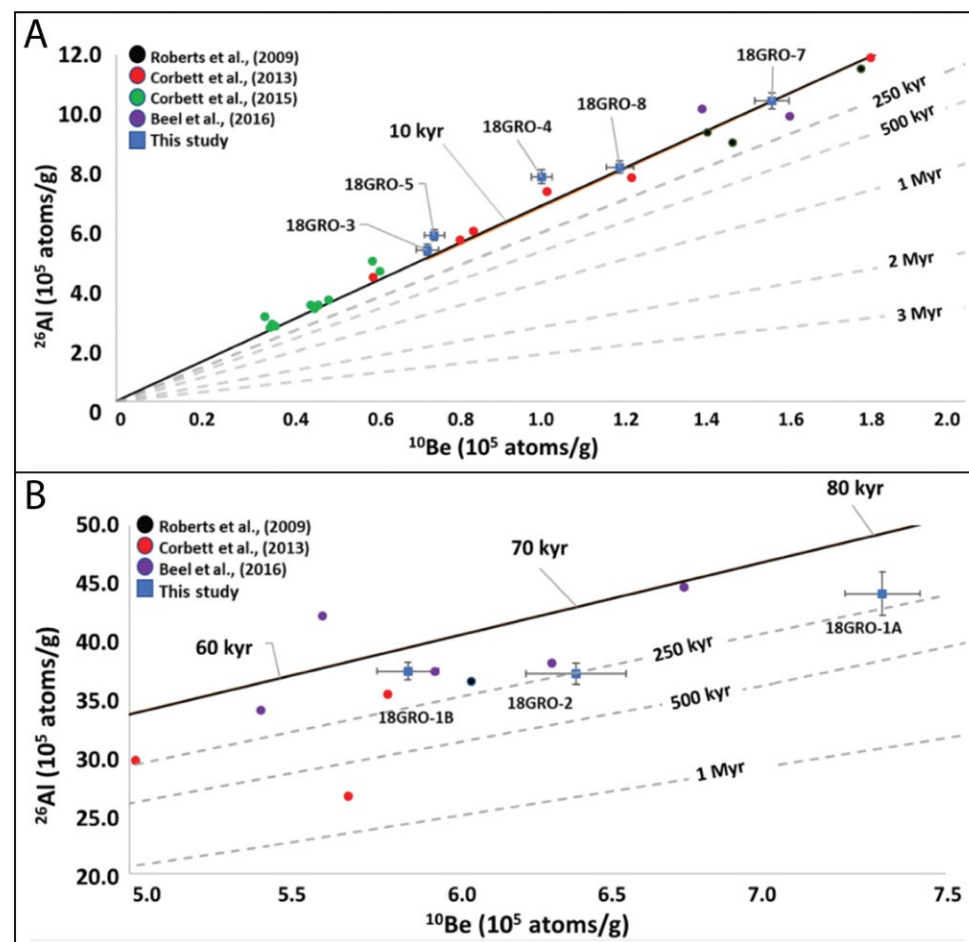


Figure 8. Burial isochron plots (see Beel et al., 2016) show  $^{26}\text{Al}$  and  $^{10}\text{Be}$  data, using a  $^{26}\text{Al}/^{10}\text{Be}$  ratio of 6.75; dashed lines are burial isochrons. (A) Samples from the western site, which overlap with constant exposure line. (B) Bedrock samples from the eastern site, which have experienced burial since initial exposure. Error bars are 1 $\sigma$ .

age as the Taserqat Moraine ( $11.6 \pm 0.4$  ka), which implies rapid deglaciation of the region at this time. Thus, the Greenland Ice Sheet likely retreated fast enough to negate any difference in ice thickness at our two study sites, causing them to become ice-free at roughly the same time. Finally, although higher in elevation, the eastern site is farther inland, and generalized ice-surface profiles indicate that

both sites would deglaciate at similar times. LGM ice probably would have been sufficiently thick to prevent continued cosmogenic nuclide accumulation through ice during the LGM, a phenomenon that has been observed at thin ice caps elsewhere in the Arctic (Pendleton et al., 2019).

Our exposure ages agree with those of Young et al. (2020) and, combined, suggest that the Sisimiut

region deglaciated at ca. 11.5 ka. We note that one of the boulders that we dated (18GRO-9) yields a  $^{10}\text{Be}$  exposure age of  $11.0 \pm 0.4$  ka, but a previous study reported a  $^{10}\text{Be}$  exposure age of  $19.6 \pm 5.2$  ka from the same boulder (GRE-1; Rinterknecht et al., 2009); however, the two ages overlap at 2 sigma. The cause of the age discrepancy may be due to improving laboratory methods like minimizing background  $^{10}\text{B}$  isobaric interference and using improved  $^{10}\text{Be}$  ion exchange chromatography for increased sample purity (Corbett et al., 2016). Winsor et al. (2015) collected nine samples from boulders for  $^{10}\text{Be}$  exposure dating at two sites close to Sisimiut. Four of five samples collected at ~585 m asl yield an average age of  $36.2 \pm 2.1$  ka with one younger age of  $17.9 \pm 0.8$  ka. Winsor et al. (2015) raised the possibility that the site remained above the LGM ice surface; in light of our results, it seems that their alternative interpretation is more likely, which is that the samples contain inheritance and the site was covered by LGM ice. Winsor et al.'s (2015) four additional  $^{10}\text{Be}$  ages, each on a boulder from ~150 m asl, average  $14.4 \pm 0.9$  ka after excluding one young age ( $10.2 \pm 0.6$  ka), which they interpreted as an outlier. These ages cannot be easily explained because they are at odds with our results and those of Young et al. (2020), but our results and the relatively younger ages from Young et al. (2020) suggest that small amounts of inherited nuclides may explain these slightly older ages.

Finally, we use likely timing of deglaciation (11.5 ka) to invert the in situ  $^{14}\text{C}$  concentration for a plausible duration of LGM ice coverage of the eastern site. Generally, in situ  $^{14}\text{C}$  becomes either fully saturated when constantly exposed or has decayed to a non-detectable level when fully buried at ~30 k.y. (Graham et al., 2019). Offshore evidence supports a glaciation in southwestern Greenland during Marine Isotope Stage 4 (MIS 4, 75–58 ka) that was more extensive than current LGM reconstructions suggest (Seidenkrantz et al., 2019). Thereafter, the Greenland Ice Sheet is generally thought to have been about as extensive as its current size throughout MIS 3 (58–27 ka) (England, 1999; Larsen et al., 2018). Thus, a plausible glacial history of the eastern site is that it became deglaciated at ca. 58 ka from an MIS 4 overriding event and subsequently remained ice free until the LGM. Following Graham

et al. (2019), we model the in situ  $^{14}\text{C}$  concentration in the samples from the eastern site assuming they were saturated with respect to  $^{14}\text{C}$  upon arrival of the ice sheet during the LGM. Next, by assuming no erosion during ice cover and re-exposure of the surfaces at 11.5 ka, we calculate the onset of ice-margin advance and surface burial to be between 19.6 ka and 14.6 ka (Fig. 9). Regardless of the exact timing and duration of LGM ice cover, our in situ  $^{14}\text{C}$  measurements that yield finite exposure ages below the saturation limit mandate that these bedrock surfaces were not exposed throughout the LGM.

## 5. CONCLUSIONS

The new results presented here point to a more extensive LGM configuration in southwestern Greenland than is currently depicted in most literature. Our comparison of marine limit values from southwestern Greenland to those from other sectors of the ice sheet suggests that an inner-shelf LGM position is incompatible with the relatively high marine limits observed at coastal sites. Our simplified crustal rebound modeling also reveals that a shelf-break LGM configuration

is more compatible with existing relative sea-level data than an ice sheet that terminated on the inner shelf. Finally, our new series of cosmogenic nuclide exposure ages supports ice cover of coastal summits and a final deglaciation age for the coast that occurred no earlier than the late Pleistocene/Holocene boundary. Thus, we favor the view that the Greenland Ice Sheet likely terminated at the continental shelf break during the LGM, with coastal deglaciation occurring just prior to ca. 11.6 ka.

Our conclusion is consistent with recent studies that place the LGM terminus position at the shelf break in the Disko Bugt and Uummannaq Fjord regions (e.g., Ó Cofaigh et al., 2013). Furthermore, the results highlight the need for direct sediment dating of the continental shelves around Greenland. Specifically, if the depositional age of the Hellefiske or Fiskebanke Moraines were known, then it would be possible to constrain the age and location of the terminus of the Greenland Ice Sheet throughout southwestern Greenland more accurately. Our evidence from southwestern Greenland joins other work suggesting that shelf break termini may have been common throughout Greenland (Fig. 1A; England, 1999; Evans et al., 2009; Larsen et al., 2018; Ó Cofaigh et al., 2013; Roberts et al.,

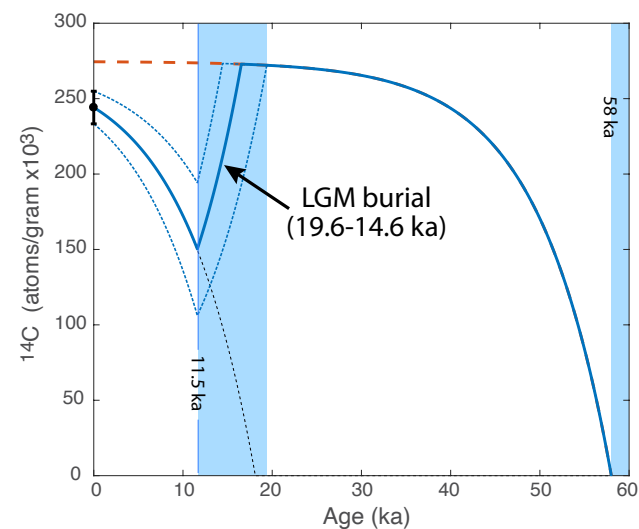


**Figure 9.** Evolution of in situ  $^{14}\text{C}$  through time for the two bedrock samples from the eastern study site is plotted. Plot shows saturation reached since an episode of deglaciation at 58 ka. To reach the average concentration of in situ  $^{14}\text{C}$  measurements from two samples (black data point with one-sigma error bar), and assuming 11.5 k.y. of exposure, the site became buried between 19.6 ka and 14.6 ka. The red dashed line shows the in situ  $^{14}\text{C}$  concentration at this site assuming no burial during the Last Glacial Maximum (LGM; surface saturation). The thin dashed line starting at 18.1 ka represents the expected age of the in situ  $^{14}\text{C}$  samples assuming a simple scenario in which the site was exposed with no inherited nuclides.

2009; Vasskog et al., 2015). Additional offshore studies and further applications of the modeling approaches taken here could test this hypothesis. If the Greenland Ice Sheet terminated at the shelf break throughout Greenland, this maximum extent would be consistent with the LGM extents of other major coastal ice sheets (Hughes et al., 2016; Mangrud et al., 1998; Margold et al., 2018).

Whereas our findings indicate that the coastal mountain summits in southwestern Greenland near Sisimiut were covered during the last glaciation, simple modeling of in situ  $^{14}\text{C}$  inventories suggests the duration of ice overriding was only  $5.5 \pm 2.5$  k.y. starting at  $17.1 \pm 2.5$  ka. Such a late maximum in ice volume is consistent with some ice-sheet modeling studies (e.g., Lecavalier et al., 2014; Buizert et al., 2018) that suggest a late LGM ice phase, perhaps correlative with Heinrich Stadial 1 (ca. 18.5–15 ka). Nevertheless, our cosmogenic nuclide measurements, modeled relative sea-level curves, and modeled ice-sheet profiles suggest that the Greenland Ice Sheet terminated at the shelf break at some point during the LGM or shortly thereafter in southwestern Greenland.

#### ACKNOWLEDGMENTS

We acknowledge Joseph Tulenko for assistance with generating maps of the study location. We thank T. Tuna and E. Bard for careful gas-source measurements at Centre de Recherche et d'Enseignement de Géosciences de l'Environnement (CEREGE). We acknowledge support by National Science Foundation Arctic System Sciences grants ARC-1504267 to J.P. Briner and E.K. Thomas and ARC-1503959 to N.E. Young. We extend thanks to Polar Field Services for field logistical support, and to two anonymous reviewers who took time to critically review this work.

#### Data and Model Code Availability

All MATLAB code and input data used to model the visco-elastic relaxation of the lithosphere for comparison to relative sea-level data is available at <http://hdl.handle.net/10477/82607>.

#### REFERENCES CITED

- Andrews, J.T., 1968a, Pattern and cause of variability of postglacial uplift and rate of uplift in Arctic Canada: *The Journal of Geology*, v. 76, p. 404–425, <https://doi.org/10.1086/627340>.
- Andrews, J.T., 1968b, Postglacial rebound in Arctic Canada: Similarity and prediction of uplift curves: *Canadian Journal of Earth Sciences*, v. 5, p. 39–47, <https://doi.org/10.1139/e68-004>.
- Andrews, J.T., 1975, *Glacial Systems: An Approach to Glaciers and their Environments*: North Scituate, Massachusetts, Duxbury Press, 191 p.
- Andrews, J.T., Buckley, J.T., and England, J.H., 1970, Late-glacial chronology and glacio-isostatic recovery, Home Bay, East Baffin Island, Canada: *Geological Society of America Bulletin*, v. 81, p. 1123–1148, [https://doi.org/10.1130/0016-7606\(1970\)81\[1123:LCAGRH\]2.0.CO;2](https://doi.org/10.1130/0016-7606(1970)81[1123:LCAGRH]2.0.CO;2).
- Balco, G., Stone, J.O., Lifton, N.A., and Dunai, T.J., 2008, A complete and easily accessible means of calculating surface exposure ages or erosion rates from  $^{10}\text{Be}$  and  $^{26}\text{Al}$  measurements: *Quaternary Geochronology*, v. 3, p. 174–195, <https://doi.org/10.1016/j.quageo.2007.12.001>.
- Bard, E., Tuna, T., Fagault, Y., Bonvalot, L., Wacker, L., Fahrni, S., and Synal, H.-A., 2015, AixMICADAS, the accelerator mass spectrometer dedicated to  $^{14}\text{C}$  recently installed in Aix-en-Provence, France: *Nuclear Instruments and Methods in Physics Research Section B: Beam Interactions with Materials and Atoms*, v. 361, p. 80–86, <https://doi.org/10.1016/j.nimb.2015.01.075>.
- Beel, C.R., Lifton, N.A., Briner, J.P., and Goehring, B.M., 2016, Quaternary evolution and ice sheet history of contrasting landscapes in Uummannaq and Sukkertoppen, western Greenland: *Quaternary Science Reviews*, v. 149, p. 248–258, <https://doi.org/10.1016/j.quascirev.2016.05.033>.
- Benn, D.I., and Hulton, N.R.J., 2010, An Excel™ spreadsheet program for reconstructing the surface profile of former mountain glaciers and ice caps: *Computers & Geosciences*, v. 36, no. 5, p. 605–610, <https://doi.org/10.1016/j.cageo.2009.09.016>.
- Bennike, O., Wagner, B., and Richter, A., 2011, Relative sea level changes during the Holocene in the Sisimiut area, south-western Greenland: *Journal of Quaternary Science*, v. 26, p. 353–361, <https://doi.org/10.1002/jqs.1458>.
- Bierman, P.R., Marsella, K.A., Patterson, C., Davis, P.T., and Caffee, M., 1999, Mid-Pleistocene cosmogenic minimum-age limits for pre-Wisconsinan glacial surfaces in southwestern Minnesota and southern Baffin Island: A multiple nuclide approach: *Geomorphology*, v. 27, p. 25–39, [https://doi.org/10.1016/S0169-555X\(98\)00088-9](https://doi.org/10.1016/S0169-555X(98)00088-9).
- Bradley, S.L., Reerink, T.J., van de Wal, R.S.W., and Helsen, M.M., 2018, Simulation of the Greenland Ice Sheet over two glacial–interglacial cycles: Investigating a sub-ice-shelf melt parameterization and relative sea level forcing in an ice-sheet–ice-shelf model: *Climate of the Past*, v. 14, p. 619–635, <https://doi.org/10.5194/cp-14-619-2018>.
- Briner, J.P., Miller, G.H., Davis, P.T., and Finkel, R.C., 2006, Cosmogenic radionuclides from fiord landscapes support differential erosion by overriding ice sheets: *Geological Society of America Bulletin*, v. 118, p. 406–420, <https://doi.org/10.1130/B25716.1>.
- Briner, J.P., Håkansson, L., and Bennike, O., 2013, The deglaciation and neoglaciation of Upernavik Isstrøm, Greenland: *Quaternary Research*, v. 80, p. 459–467, <https://doi.org/10.1016/j.yqres.2013.09.008>.
- Buizert, C., Keisling, B.A., Box, J.E., He, F., Carlson, A.E., Sinclair, G., and DeConto, R.M., 2018, Greenland-wide seasonal temperatures during the last deglaciation: *Geophysical Research Letters*, v. 45, p. 1905–1914, <https://doi.org/10.1002/2017GL075601>.
- Corbett, L.B., Bierman, P.R., Graly, J.A., Neumann, T.A., and Rood, D.H., 2013, Constraining landscape history and glacial erosivity using paired cosmogenic nuclides in Upernavik, northwest Greenland: *Geological Society of America Bulletin*, v. 125, p. 1539–1553, <https://doi.org/10.1130/B30813.1>.
- Corbett, L.B., Bierman, P.R., and Rood, D.H., 2016, An approach for optimizing in situ cosmogenic  $^{10}\text{Be}$  sample preparation: *Quaternary Geochronology*, v. 33, p. 24–34, <https://doi.org/10.1016/j.quageo.2016.02.001>.
- Corbett, L.B., Bierman, P.R., Rood, D.H., Caffee, M.W., Lifton, N.A., and Thomas E. Woodruff, T.E., 2017, Cosmogenic  $^{26}\text{Al}/^{10}\text{Be}$  surface production ratio in Greenland: *Geophysical Research Letters*, v. 44, no. 3, p. 1350–1359, <https://doi.org/10.1002/2016GL071276>.
- Dalton, A.S., Margold, M., Stokes, C.R., Tarasov, L., Dyke, A.S., and Adams, R.S., 2020, An updated radiocarbon-based ice margin chronology for the last deglaciation of the North American Ice Sheet Complex: *Quaternary Science Reviews*, v. 234, <https://doi.org/10.1016/j.quascirev.2020.106223>.
- Dowdeswell, J.A., Hogan, K.A., Ó Cofaigh, C., Fugelli, E.M.G., Evans, J., and Noormets, R., 2014, Late Quaternary ice flow in a West Greenland fjord and cross-shelf trough system: Submarine landforms from Rink Isbrae to Uummannaq shelf and slope: *Quaternary Science Reviews*, v. 92, p. 292–309, <https://doi.org/10.1016/j.quascirev.2013.09.007>.
- Downs, J., Johnson, J., Briner, J., Young, N., Lesnek, A., and Cuzzone, J., 2020, Western Greenland ice sheet retreat history reveals elevated precipitation during the Holocene thermal maximum: *The Cryosphere*, v. 14, p. 1121–1137, <https://doi.org/10.5194/tc-14-1121-2020>.
- Dyke, A.S., 2004, An outline of North American deglaciation with emphasis on central and northern Canada, in Ehlers, J., and Gibbard, P.L., eds., *Quaternary Glaciations—Extent and Chronology, Part II: North America*: Amsterdam, The Netherlands, Elsevier, Developments in Quaternary Sciences, v. 2, p. 373–424, [https://doi.org/10.1016/S1571-0866\(04\)80209-4](https://doi.org/10.1016/S1571-0866(04)80209-4).
- Dyke, A., Dredge, L., and Hodgson, D., 2005, North American deglacial marine- and lake-limit surfaces: *Géographie Physique et Quaternaire*, v. 59, p. 155–185, <https://doi.org/10.7202/014753ar>.
- England, J., 1999, Coalescent Greenland and Innuitan ice during the Last Glacial Maximum: Revising the Quaternary of the Canadian High Arctic: *Quaternary Science Reviews*, v. 18, p. 421–456, [https://doi.org/10.1016/S0277-3791\(98\)00070-5](https://doi.org/10.1016/S0277-3791(98)00070-5).
- Evans, J., Cofaigh, C.Ó., Dowdeswell, J.A., and Wadhams, P., 2009, Marine geophysical evidence for former expansion and flow of the Greenland Ice Sheet across the north-east Greenland continental shelf: *Journal of Quaternary Science*, v. 24, p. 279–293, <https://doi.org/10.1002/jqs.1231>.
- Fleming, K., and Lambeck, K., 2004, Constraints on the Greenland Ice Sheet since the Last Glacial Maximum from sea-level observations and glacial-rebound models: *Quaternary Science Reviews*, v. 23, p. 1053–1077, <https://doi.org/10.1016/j.quascirev.2003.11.001>.
- Fleming, K., Johnston, P., Zwartz, D., Yokoyama, Y., Lambeck, K., and Chappell, J., 1998, Refining the eustatic sea-level curve since the Last Glacial Maximum using far- and intermediate-field sites: *Earth and Planetary Science Letters*, v. 163, p. 327–342, [https://doi.org/10.1016/S0012-821X\(98\)00198-8](https://doi.org/10.1016/S0012-821X(98)00198-8).
- Forman, S.L., 1990, Post-glacial relative sea-level history of northwestern Spitsbergen, Svalbard: *Geological Society of America Bulletin*, v. 102, p. 1580–1590, [https://doi.org/10.1130/0016-7606\(1990\)102<1580:PGRSLH>2.3.CO;2](https://doi.org/10.1130/0016-7606(1990)102<1580:PGRSLH>2.3.CO;2).

- Funder, S., and Hansen, L., 1996, The Greenland ice sheet—A model for its culmination and decay during and after the last glacial: *Bulletin of the Geological Society of Denmark*, v. 42, no. 2, p. 137–152, <https://doi.org/10.37570/bgsd-1995-42-12>.
- Funder, S., Kjeldsen, K.K., Kjær, K.H., and Ó Cofaigh, C., 2011, Chapter 50—The Greenland Ice Sheet during the past 300,000 years: A Review, in Ehlers, J., Gibbard, P.L., and Hughes, P.D., eds., *Quaternary Glaciations—Extent and Chronology, A Closer Look*: Amsterdam, The Netherlands, Developments in Quaternary Sciences, v. 15, p. 699–713, <https://doi.org/10.1016/B978-0-444-53447-7.00050-7>.
- Graham, B.L., Briner, J.P., Schweinsberg, A.D., Lifton, N.A., and Bennike, O., 2019, New in situ  $^{14}\text{C}$  data indicate the absence of nunataks in west Greenland during the Last Glacial Maximum: *Quaternary Science Reviews*, v. 225, <https://doi.org/10.1016/j.quascirev.2019.105981>.
- Håkansson, L., Briner, B., Alexanderson, H., Aldahan, A., and Possnert, G., 2007,  $^{10}\text{Be}$  ages from central east Greenland constrain the extent of the Greenland ice sheet during the Last Glacial Maximum: *Quaternary Science Reviews*, v. 26, no. 19–21, p. 2316–2321, <http://doi.org/10.1016/j.quascirev.2007.08.001>.
- Halsted, C.T., Bierman, P.R., and Balco, G., 2021, Empirical evidence for latitude and altitude variation of the in situ cosmogenic  $^{26}\text{Al}/^{10}\text{Be}$  production ratio: *Geosciences*, v. 11, no. 10, p. 402, <https://doi.org/10.3390/geosciences11100402>.
- He, F., Shakun, J.D., Clark, P.U., Carlson, A.E., Liu, Z., Otto-Bliesner, B.L., and Kutzbach, J.E., 2013, Northern Hemisphere forcing of Southern Hemisphere climate during the last deglaciation: *Nature*, v. 494, p. 81–85, <https://doi.org/10.1038/nature11822>.
- Hogan, K.A., Ó Cofaigh, C., Jennings, A.E., Dowdeswell, J.A., and Hiemstra, J.F., 2016, Deglaciation of a major palaeo-ice stream in Disko Trough, West Greenland: *Quaternary Science Reviews*, v. 147, p. 5–26, <https://doi.org/10.1016/j.quascirev.2016.01.018>.
- Hughes, A.L.C., Gyllencreutz, R., Lohne, Ø.S., Mangerud, J., and Svendsen, J.I., 2016, The last Eurasian ice sheets—A chronological database and time-slice reconstruction, DATED-1: *Boreas*, v. 45, p. 1–45, <https://doi.org/10.1111/bor.12142>.
- Jennings, A.E., Andrews, J.T., Ó Cofaigh, C., St. Onge, G., Sheldon, C., and Belt, S.T., 2017, Ocean forcing of Ice Sheet retreat in central west Greenland from LGM to the early Holocene: *Earth and Planetary Science Letters*, v. 472, p. 1–13, <https://doi.org/10.1016/j.epsl.2017.05.007>.
- Kelly, M., 1980, Preliminary investigations of the Quaternary of Melville Bugt and Dundas, north-west Greenland: *Gronlands Geologiske Undersøgelse Rapport*, v. 100, p. 33–38, <https://doi.org/10.34194/rappgu.v100.7691>.
- Kelly, M., and Bennike, O., 1985, Quaternary geology of parts of central and western North Greenland: A preliminary account: *Gronlands Geologiske Undersøgelse*, v. 126, p. 111–116, <https://doi.org/10.34194/rappgu.v126.7917>.
- Lal, D., 1991, Cosmic ray labeling of erosion surfaces: In situ nuclide production rates and erosion models: *Earth and Planetary Science Letters*, v. 104, p. 424–439, [https://doi.org/10.1016/0012-821X\(91\)90220-C](https://doi.org/10.1016/0012-821X(91)90220-C).
- Lambeck, K., Rouby, H., Purcell, A., Sun, Y., and Sambridge, M., 2014, Sea level and global ice volumes from the Last Glacial Maximum to the Holocene: *Proceedings of the National Academy of Sciences of the United States of America*, v. 111, p. 15,296–15,303, <https://doi.org/10.1073/pnas.1411762111>.
- Lamp, J.L., Young, N.E., Koffman, T., Schimmelpennig, I., Tuna, T., Bard, E., and Schaefer, J.M., 2019, Update on the cosmogenic in situ  $^{14}\text{C}$  laboratory at the Lamont-Doherty Earth Observatory: *Nuclear Instruments & Methods in Physics Research Section B: Beam Interactions with Materials and Atoms*, v. 456, p. 157–162, <https://doi.org/10.1016/j.nimb.2019.05.064>.
- Larsen, N.K., Levy, L.B., Carlson, A.E., Buizert, C., Olsen, J., and Strunk, A., 2018, Instability of the Northeast Greenland Ice Stream over the last 45,000 years: *Nature Communications*, v. 9, p. 1–8, <https://doi.org/10.1038/s41467-018-04312-7>.
- Lecavalier, B.S., Milne, G.A., Simpson, M.J.R., Wake, L., Huybrechts, P., and Tarasov, L., 2014, A model of Greenland ice sheet deglaciation constrained by observations of relative sea level and ice extent: *Quaternary Science Reviews*, v. 102, p. 54–84, <https://doi.org/10.1016/j.quascirev.2014.07.018>.
- Lesnek, A.J., Briner, J.P., Young, N.E., and Cuzzone, J.K., 2020, Maximum Southwest Greenland Ice Sheet recession in the early Holocene: *Geophysical Research Letters*, v. 47, <https://doi.org/10.1029/2019GL083164>.
- Long, A.J., Woodroffe, S.A., Dawson, S., Roberts, D.H., and Bryant, C.L., 2009, Late Holocene relative sea level rise and the Neoglacial history of the Greenland ice sheet: *Journal of Quaternary Science*, v. 24, p. 345–359, <https://doi.org/10.1002/jqs.1235>.
- Long, A.J., Woodroffe, S.A., Roberts, D.H., and Dawson, S., 2011, Isolation basins, sea-level changes and the Holocene history of the Greenland Ice Sheet: *Quaternary Science Reviews*, v. 30, p. 3748–3768, <https://doi.org/10.1016/j.quascirev.2011.10.013>.
- Mangerud, J., Dokken, T., Hebbeln, D., Heggen, B., Ingólfsson, Ó., and Landvik, J.Y., 1998, Fluctuations of the Svalbard-Barents Sea Ice Sheet during the Last 150,000 years: *Quaternary Science Reviews*, v. 17, p. 11–42, [https://doi.org/10.1016/S0277-3791\(97\)00069-3](https://doi.org/10.1016/S0277-3791(97)00069-3).
- Margold, M., Stokes, C.R., and Clark, C.D., 2018, Reconciling records of ice streaming and ice margin retreat to produce a palaeogeographic reconstruction of the deglaciation of the Laurentide Ice Sheet: *Quaternary Science Reviews*, v. 189, p. 1–30, <https://doi.org/10.1016/j.quascirev.2018.03.013>.
- Martinez, Z., Klemann, V., van der Wal, W., Riva, R.E.M., Spada, G., Sun, Y., Melini, D., Kachuck, S.B., Barletta, V., Simon, K., G.A., and James, T.S., 2018, A benchmark study of numerical implementations of the sea level equation in GIA modelling: *Geophysical Journal International*, v. 215, no. 1, p. 389–414, <https://doi.org/10.1093/gji/ggy280>.
- Meinesz, F.A., 1937, The determination of the earth's plasticity from the post-glacial uplift of Scandinavia: *Isostatic adjustment: Proceedings of the Koninklijke Nederlandse Akademie van Wetenschappen*, v. 40, p. 654–662.
- Morlighem, M., Williams, C.N., Rignot, E., An, L., Arndt, J.E., Bamber, J.L., Catania, G., Chauché, N., Dowdeswell, J.A., Dorschel, B., Fenty, I., Hogan, K., Howat, I., Hubbard, A., Jakobsson, M., Jordan, T.M., Kjeldsen, K.K., Millan, R., Mayer, L., Mouginot, J., Noël, B.P.Y., O'Cofoigh, C., Palmer, S., Rysgaard, S., Seroussi, H., Siegert, M.J., Slabon, P., Straneo, F., van den Broeke, M.R., Weinrebe, W., Wood, M., and Zinglens, K.B., 2017, *BedMachine v3*: Complete bed topography and ocean bathymetry mapping of Greenland from multibeam echo sounding combined with mass conservation: *Geophysical Research Letters*, v. 44, no. 21, p. 11,051–11,061, <https://doi.org/10.1002/2017GL074954>.
- Newton, A.M.W., Knutz, P.C., Huuse, M., Gannon, P., Brocklehurst, S.H., Clausen, O.R., and Gong, Y., 2017, Ice stream reorganization and glacial retreat on the northwest Greenland shelf: *Geophysical Research Letters*, v. 44, p. 7826–7835, <https://doi.org/10.1002/2017GL073690>.
- Ó Cofaigh, C., Dowdeswell, J.A., Evans, J., Kenyon, N.H., Taylor, J., Mienert, J., and Wilken, M., 2004, Timing and significance of glacially influenced mass-wasting in the submarine channels of the Greenland Basin: *Marine Geology*, v. 207, p. 39–54, <https://doi.org/10.1016/j.margeo.2004.02.009>.
- Ó Cofaigh, C., Dowdeswell, J.A., Jennings, A.E., Hogan, K.A., Kilfeather, A., and Hiemstra, J.F., 2013, An extensive and dynamic ice sheet on the West Greenland shelf during the last glacial cycle: *Geology*, v. 41, p. 219–222, <https://doi.org/10.1130/G33759.1>.
- Peltier, W.R., 1998, Postglacial variations in the level of the sea: Implications for climate dynamics and solid-Earth geophysics: *Reviews of Geophysics*, v. 36, p. 603–689, <https://doi.org/10.1029/98RG02638>.
- Pendleton, S.L., Miller, G.H., Lifton, N., Lehman, S.J., Southon, J., Crump, S.E., and Anderson, R.S., 2019, Rapidly receding Arctic Canada glaciers revealing landscapes continuously ice-covered for more than 40,000 years: *Nature Communications*, v. 10, p. 1–8, <https://doi.org/10.1038/s41467-019-08307-w>.
- Rinterknecht, V., Gorokhovich, Y., Schaefer, J., and Caffee, M., 2009, Preliminary  $^{10}\text{Be}$  chronology for the last deglaciation of the western margin of the Greenland Ice Sheet: *Journal of Quaternary Science*, v. 24, p. 270–278, <https://doi.org/10.1002/jqs.1226>.
- Roberts, D.H., Long, A.J., Schnabel, C., Davies, B.J., Xu, S., Simpson, M.J.R., and Huybrechts, P., 2009, Ice sheet extent and early deglacial history of the south-western sector of the Greenland Ice Sheet: *Quaternary Science Reviews*, v. 28, p. 2760–2773, <https://doi.org/10.1016/j.quascirev.2009.07.002>.
- Ruskeeniemi, T., Engström, J., Lehtimäki, J., Vanhala, H., Korhonen, K., Kontula, A., Lijedahl, L.C., Näslund, J.O., and Petterson, R., 2018, Subglacial permafrost evidencing re-advance of the Greenland Ice Sheet over frozen ground: *Quaternary Science Reviews*, v. 199, p. 174–187, <https://doi.org/10.1016/j.quascirev.2018.09.002>.
- Seidenkrantz, M.-S., Kuijpers, A., Olsen, O., Pearce, C., Lindblom, S., Ploug, J., Przybylo, P., and Snowball, I., 2019, Southwest Greenland shelf glaciation during MIS 4 more extensive than during the Last Glacial Maximum: *Scientific Reports*, v. 9, no. 1, p. 1–11, <https://doi.org/10.1038/s41598-019-51983-3>.
- Søndergaard, A.S., Larsen, N.K., Lecavalier, B.S., Olsen, J., Fitzpatrick, N.P., Kjær, K.H., and Khan, S.A., 2020, Early Holocene collapse of marine-based ice in northwest Greenland triggered by atmospheric warming: *Quaternary Science Reviews*, v. 239, <https://doi.org/10.1016/j.quascirev.2020.106360>.
- Spada, G., Barletta, V.R., Klemann, V., Riva, R.E.M., Martinez, Z., Gasperini, P., Lund, B., Wolf, D., Vermeersen, L.L.A., and King, M.A., 2011, A benchmark study for glacial isostatic adjustment codes: *Geophysical Journal International*, v. 185, no. 1, p. 106–132, <https://doi.org/10.1111/j.1365-246X.2011.04952.x>.
- Steffen, R., Audet, P., and Lund, B., 2018, Weakened lithosphere beneath Greenland inferred from effective elastic thickness:

- A hot spot effect?: *Geophysical Research Letters*, v. 45, p. 4733–4742, <https://doi.org/10.1029/2017GL076885>.
- Stone, J.O., 2000, Air pressure and cosmogenic isotope production: *Journal of Geophysical Research: Solid Earth*, v. 105, p. 23,753–23,759, <https://doi.org/10.1029/2000JB900181>.
- Strunk, A., Faurischou Knudsen, M., Egholm, D.L., Jansen, J.D., Levy, L.B., Jacobsen, B.H., and Larsen, N.K., 2017, One million years of glaciation and denudation history in west Greenland: *Nature Communications*, v. 8, no. 1, p. 1–8, <https://doi.org/10.1038/ncomms14199>.
- Tarasov, L., and Peltier, W.R., 2004, A geophysically constrained large ensemble analysis of the deglacial history of the North American ice-sheet complex: *Quaternary Science Reviews*, v. 23, p. 359–388, <https://doi.org/10.1016/j.quascirev.2003.08.004>.
- Tuna, T., Fagault, Y., Bonvalot, L., Capano, M., and Bard, W., 2018, Development of small CO<sub>2</sub> gas measurements with AixMICADAS: Nuclear Instruments and Methods in Physics Research Section B: Beam Interactions with Materials and Atoms, v. 437, p. 93–97, <https://doi.org/10.1016/j.nimb.2018.09.012>.
- Turcotte, D.L., and Schubert, G., 2002, *Geodynamics*: Cambridge, UK, Cambridge University Press, 456 p., <https://doi.org/10.1017/CBO9780511807442>.
- van der Veen, C.J., 2013, *Fundamentals of Glacier Dynamics*: Boca Raton, Florida, CRC Press, 403 p., <https://doi.org/10.1201/b14059>.
- Vasskog, K., Langebroek, P.M., Andrews, J.T., Nilsen, J.E.Ø., and Nesje, A., 2015, The Greenland Ice Sheet during the last glacial cycle: Current ice loss and contribution to sea-level rise from a palaeoclimatic perspective: *Earth-Science Reviews*, v. 150, p. 45–67, <https://doi.org/10.1016/j.earscirev.2015.07.006>.
- Wake, L.M., Lecavalier, B.S., and Bevis, M., 2016, Glacial isostatic adjustment (GIA) in Greenland: A review: *Current Climate Change Reports*, v. 2, p. 101–111, <https://doi.org/10.1007/s40641-016-0040-z>.
- Weidick, A., and Bennike, O., 2007, Quaternary glaciation history and glaciology of Jakobshavn Isbræ and the Disko Bugt region, West Greenland: A review: *Geological Survey of Denmark and Greenland Bulletin*, v. 14, p. 1–78.
- Winsor, K., Carlson, A.E., Caffee, M.W., and Rood, D.H., 2015, Rapid last-deglacial thinning and retreat of the marine-terminating southwestern Greenland ice sheet: *Earth and Planetary Science Letters*, v. 426, p. 1–12, <https://doi.org/10.1016/j.epsl.2015.05.040>.
- Young, N.E., and Briner, J.P., 2015, Holocene evolution of the western Greenland Ice Sheet: Assessing geophysical ice-sheet models with geological reconstructions of ice-margin change: *Quaternary Science Reviews*, v. 114, p. 1–17, <https://doi.org/10.1016/j.quascirev.2015.01.018>.
- Young, N.E., Schaefer, J.M., Briner, J.P., and Goehring, B.M., 2013, A <sup>10</sup>Be production-rate calibration for the Arctic: *Journal of Quaternary Science*, v. 28, no. 5, p. 515–526.
- Young, N.E., Schaefer, J.M., Goehring, B., Lifton, N., Schimmelpennig, I., and Briner, J.P., 2014, West Greenland and global in situ <sup>14</sup>C production-rate calibrations: *Journal of Quaternary Science*, v. 29, no. 5, p. 401–406, <https://doi.org/10.1002/jqs.2717>.
- Young, N.E., Lamp, J., Koffman, T., Briner, J.P., Schaefer, J., and Gjermundsen, E.F., 2018, Deglaciation of coastal southwestern Spitsbergen dated with in situ cosmogenic <sup>10</sup>Be and <sup>14</sup>C measurements: *Journal of Quaternary Science*, v. 33, p. 763–776, <https://doi.org/10.1002/jqs.3058>.
- Young, N.E., Briner, J.P., Miller, G.H., Lesnek, A.J., Crump, S.E., Thomas, E.K., Pendleton, S.L., Cuzzone, J., Lamp, J., Zimmerman, S., and Caffee, M., 2020, Deglaciation of the Greenland and Laurentide ice sheets interrupted by glacier advance during abrupt coolings: *Quaternary Science Reviews*, v. 229, <https://doi.org/10.1016/j.quascirev.2019.106091>.
- Young, N.E., Lesnek, A.J., Cuzzone, J.K., Briner, J.P., Badgley, J.A., Balter-Kennedy, A., Graham, B.L., Cluett, A., Lamp, J.L., Schwartz, R., Tuna, T., Bard, E., Caffee, M.W., Zimmerman, S.R.H., and Schaefer, J.M., 2021, In situ cosmogenic <sup>10</sup>Be-<sup>14</sup>C-<sup>26</sup>Al measurements from recently deglaciated bedrock as a new tool to decipher changes in Greenland Ice Sheet size: *Climate of the Past*, v. 17, p. 419–450, <https://doi.org/10.5194/cp-17-419-2021>.
- Zweck, C., and Huybrechts, P., 2005, Modeling of the northern hemisphere ice sheets during the last glacial cycle and glaciological sensitivity: *Journal of Geophysical Research: Atmospheres*, v. 110, <https://doi.org/10.1029/2004JD005489>.